Electronic Supplementary Material (ESI) for Journal of Materials Chemistry C.

Supplementary Information

714 nm Emission with 12.25% Efficiency from Iridium Complexes with low iridium content by the Strategy of Rigid Coordination Core and Amplifying Shell

Li Wang,[#a] Sai Wang,[#a] Caifa You,[b] Xiang Chang,[a] Jingwei Huang,[a] Weiqiong Zhen,[a] Hu Zhang,[a] Xiangqin Gan,[a] Xiugang Wu[a*] and Weiguo Zhu[a*]

[a] School of Materials Science and Engineering, Jiangsu Engineering Laboratory of Light-Electricity-Heat Energy-Converting Materials and Applications, Jiangsu Key Laboratories of Environment-Friendly Polymers, National Experimental Demonstration Center for Materials Science and Engineering, Changzhou University, Changzhou 213164, P. R. China.

[b] Department of Materials Sciences and Engineering, City University of Hong Kong, Hong Kong SAR, P. R. China

Email addresses: zhuwg18@126.com (W. G. Zhu)

Contents of Figures and Tables

Figure S16.MALDI-TOF-MS spectrum of (^{t}BuTPA-DBPz)$_2$Ir(acac).

Table S1. TD-DFT results for complexes based on their optimized S_0 geometries

Table S2. Excited state properties of (DBPz)$_2$Ir(dpm) obtained from TD-DFT calculations carried out at the ground state(S_0) geometry.

Table S3. Excited state properties of (^{t}BuTPA-DBPz)$_2$Ir(acac) obtained from TD-DFT calculations carried out at the ground state(S_0) geometry.

Table S4 EL performance of the (^{t}BuTPA-DBPz)$_2$Ir(acac) doped devices at different dopant ratios of 1.0 wt%, 4.0 wt% and 8.0 wt%.

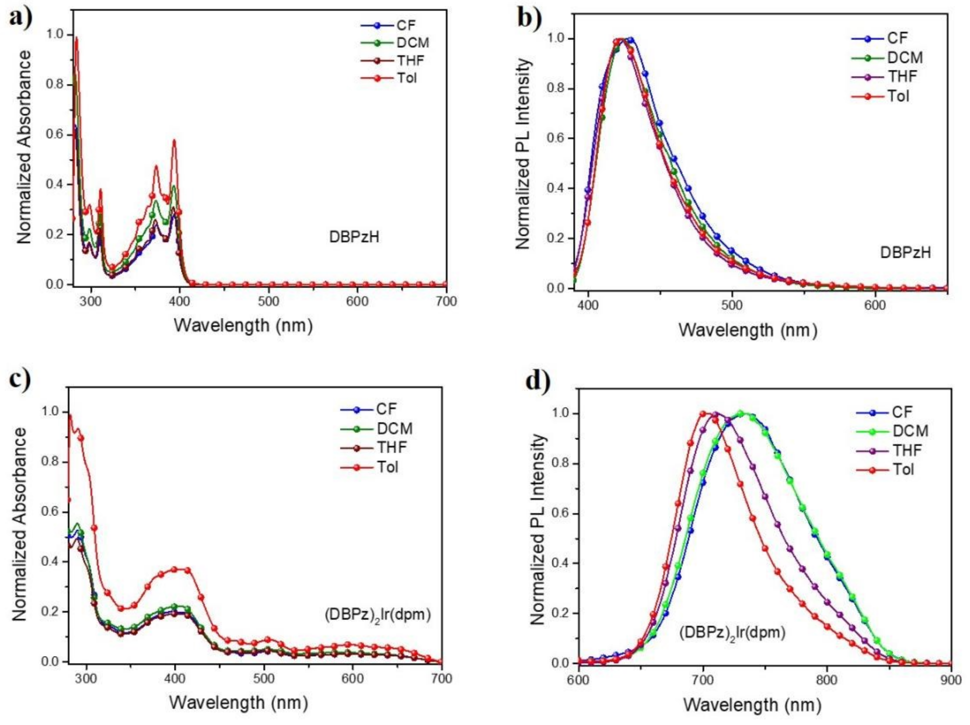

Figure S1. UV-Vis and PL spectra of DBPzH (a,b) and (DBPz)$_2$Ir(dpm) (c, d) at RT in different solvents under same measurement conditions, Ex = 470 nm

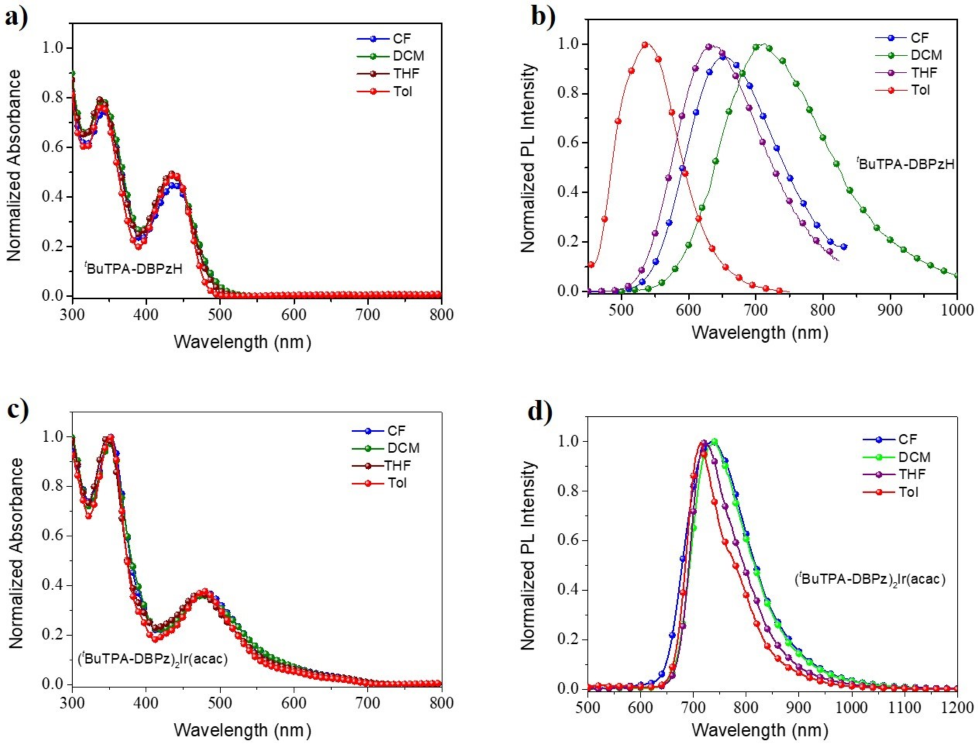

Figure S2. UV-Vis and PL spectra of ^{t}BuTPA-DBPzH (a,b) and (^{t}BuTPABPz)$_2$Ir(acac) (c,d) at RT in different solvents under same measurement conditions, Ex = 470 nm.

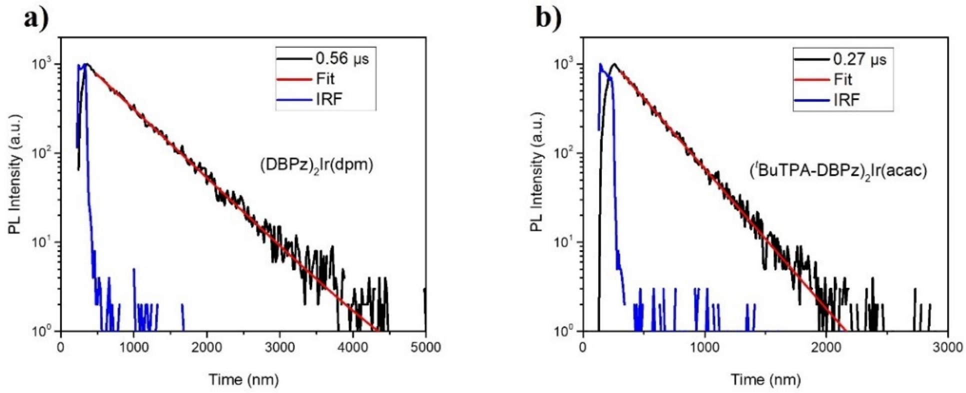

Figure S3. Decay curves of (DBPz)$_2$Ir(dpm) and (^{t}BuTPA-DBPz)$_2$Ir(acac) in a deoxygenated DCM solution.

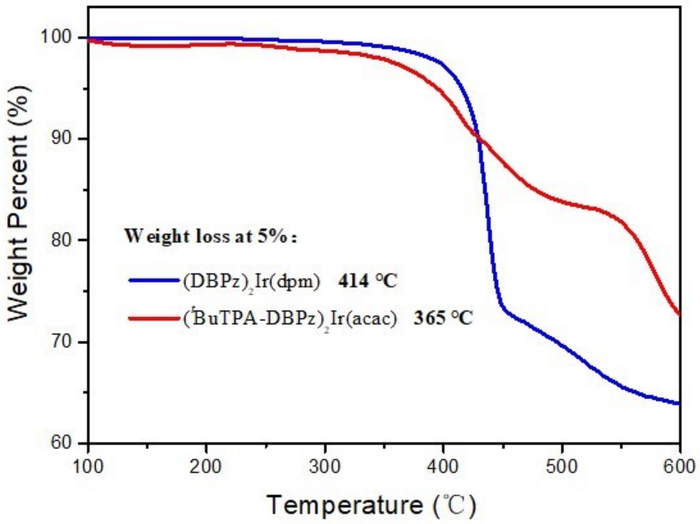

Figure S4. TGA curves of (DBPz)$_2$Ir(dpm) and (^{t}BuTPA-DBPz)$_2$Ir(acac) under N_2 with a rate of 20 °C/min.

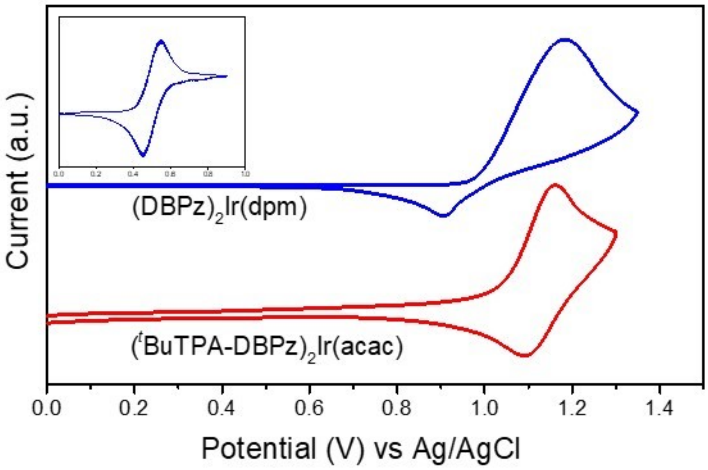

Figure S5. Cyclic voltammograms of (DBPz)$_2$Ir(dpm) and (^{t}BuTPA-DBPz)$_2$Ir(acac) in CH_3CN solutions.

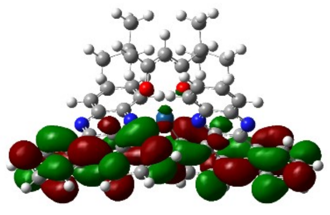	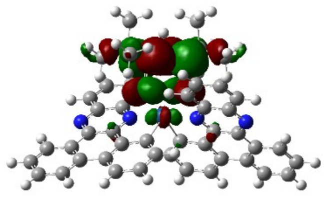	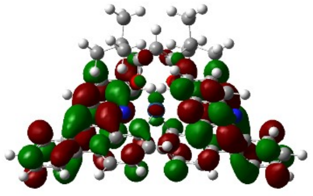
LUMO+5	LUMO+4	LUMO+3
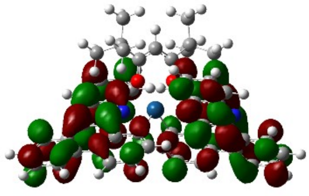	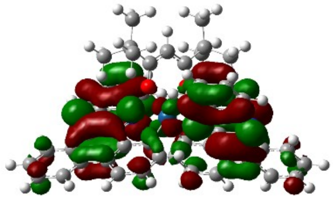	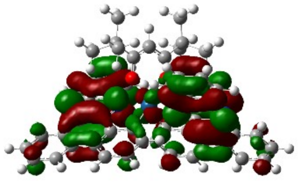
LUMO+2	LUMO+1	LUMO
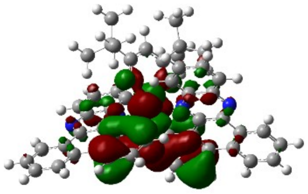	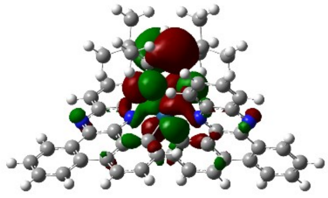	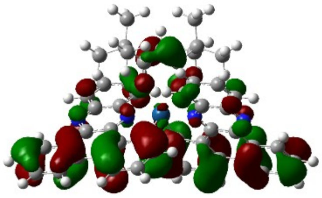
HOMO	HOMO-1	HOMO-2
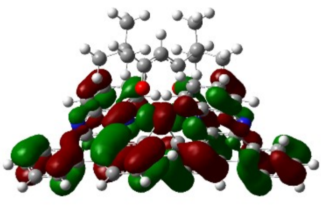	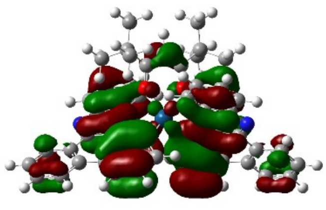	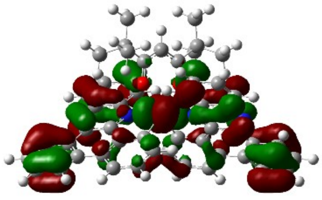

HOMO-3	HOMO-4	HOMO-5

Figure S6. Selected molecular orbital diagrams of complex (DBPz)$_2$Ir(dpm) based on its optimized triplet state geometry.

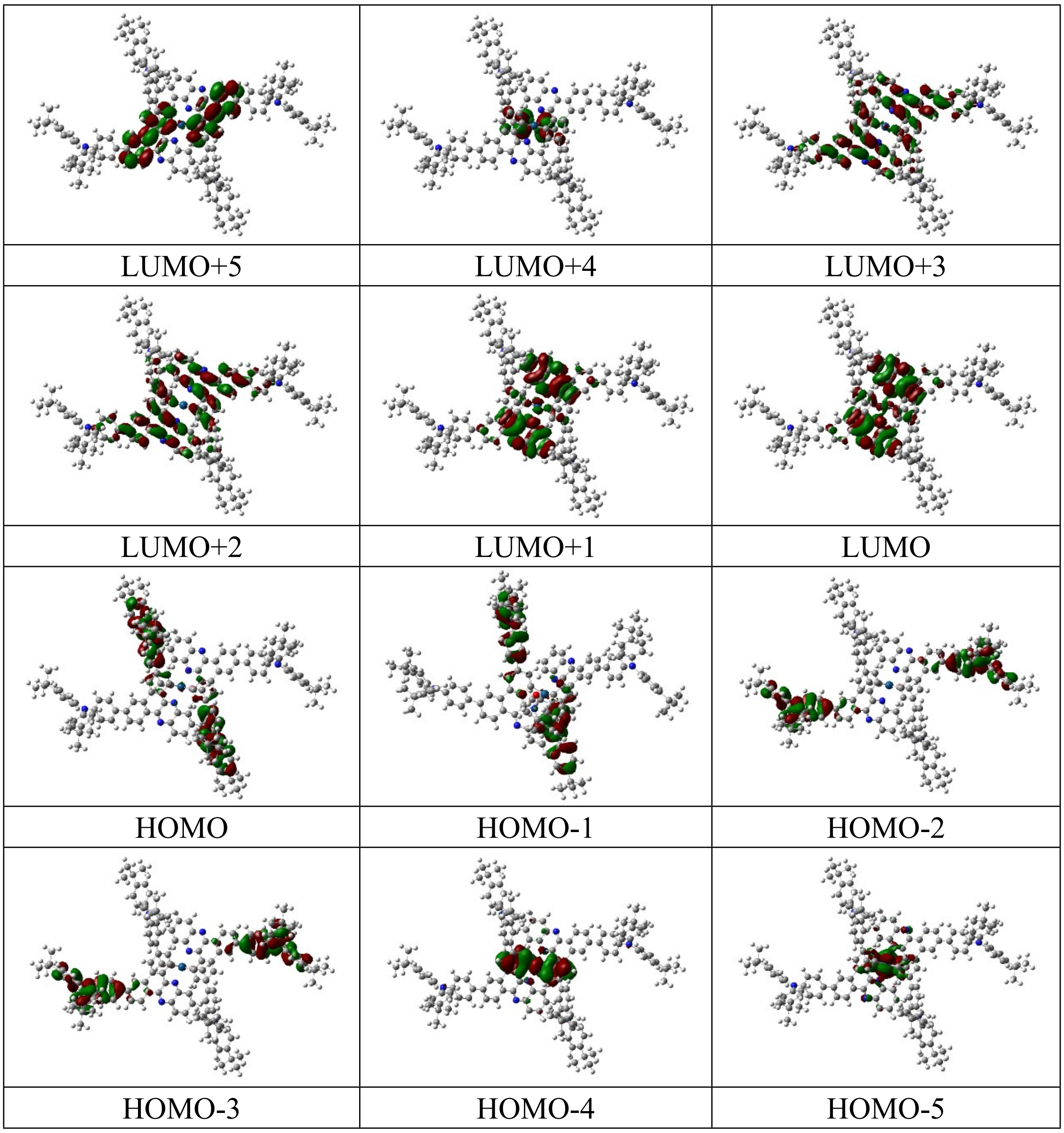

LUMO+5 LUMO+4 LUMO+3

LUMO+2 LUMO+1 LUMO

HOMO HOMO-1 HOMO-2

HOMO-3 HOMO-4 HOMO-5

Figure S7. Selected molecular orbital diagrams of complex (^{t}BuTPA-DBPz)$_2$Ir(acac) based on its optimized triplet state geometry.

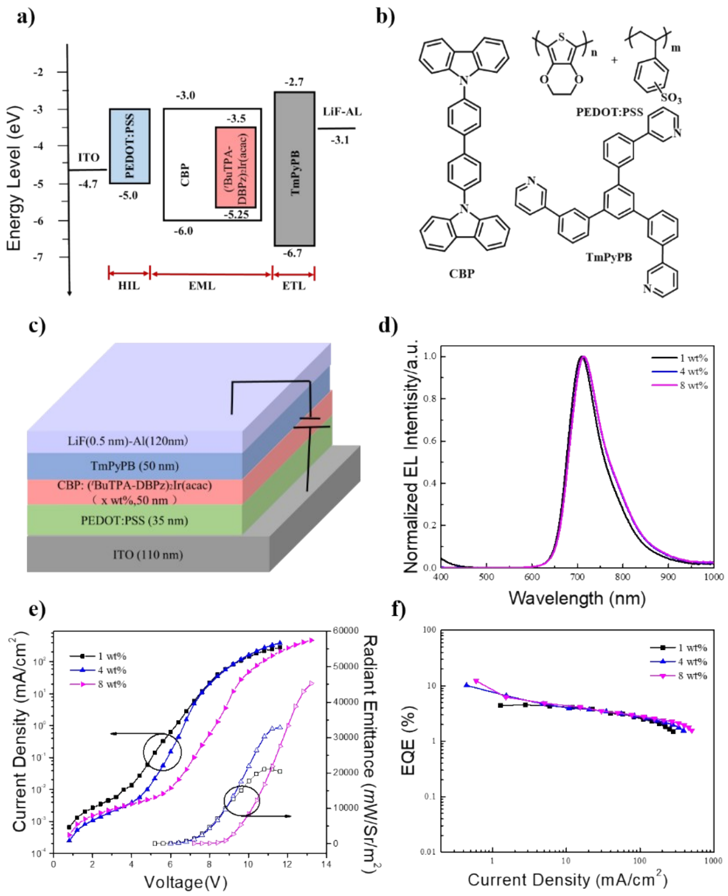

Figure S8. (a) Energy level diagram of the OLEDs, (b) Chemical structures of the relevant transport materials, (c) Diagram of the device structure (50nm), (d) EL spectra, (e) current density–voltage–luminance (*J*–*V*–*L*) curves and (f) *EQE*-current density curves in the (^{t}BuTPA-DBPz)$_2$Ir(acac) doped OLEDs with various doping concentrations from 1.0 wt%, 4.0 wt% and 8.0 wt%.

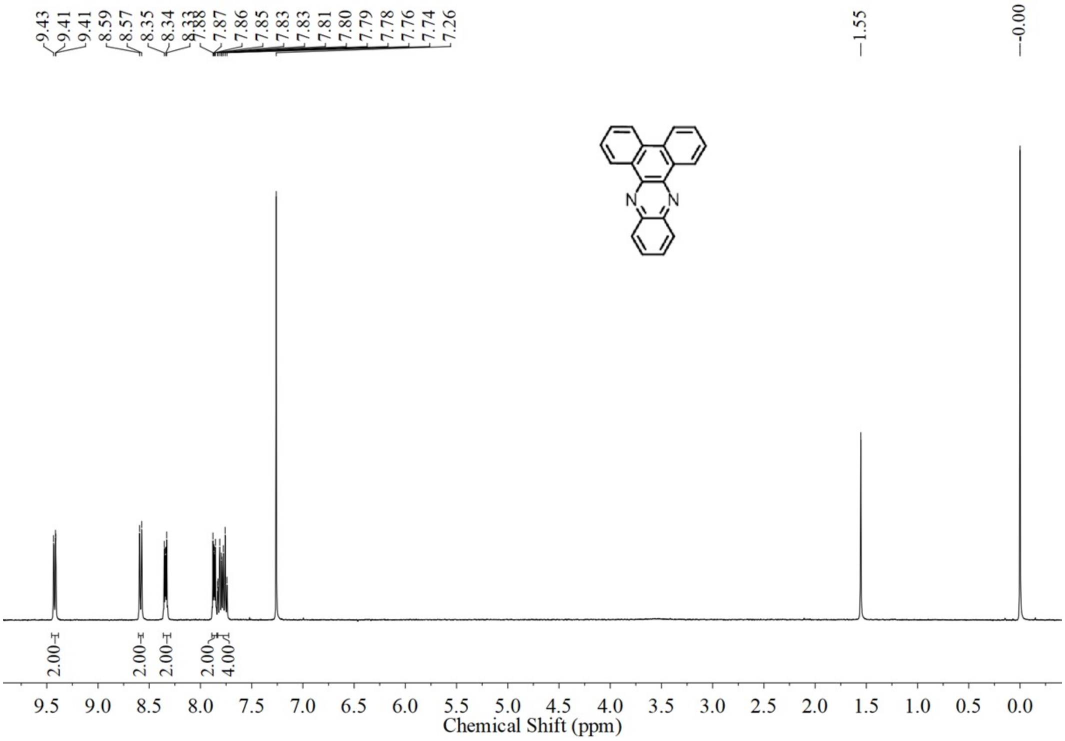

Figure S9. ^{1}H-NMR spectrum of DBPzH.

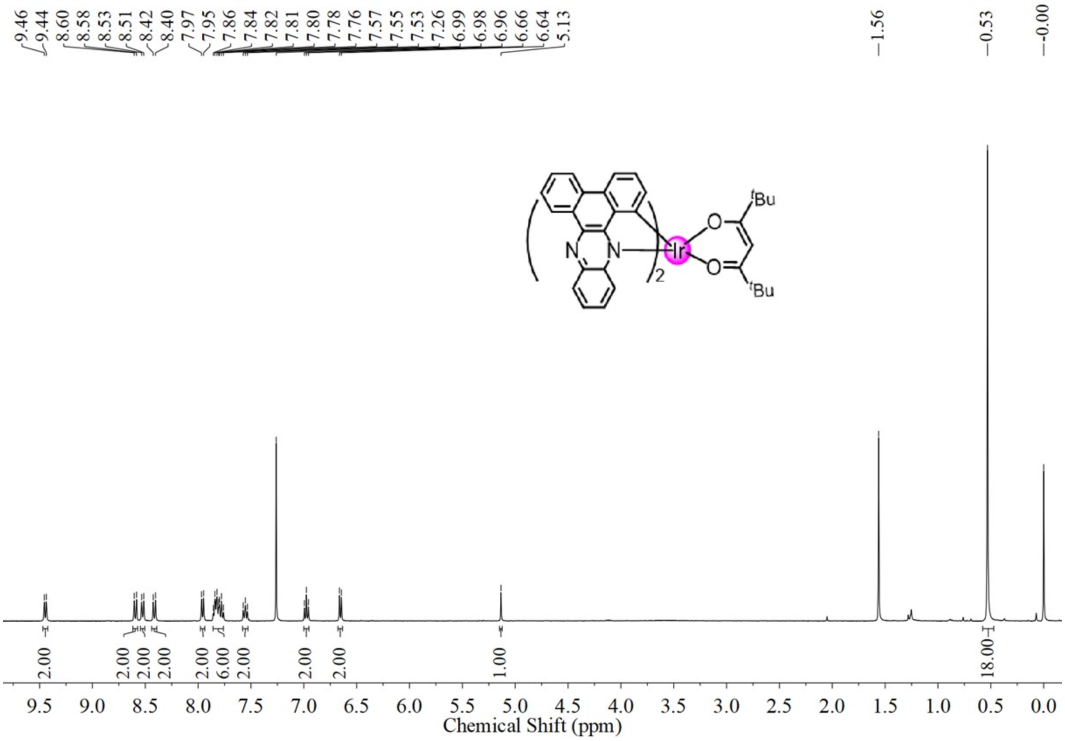

Figure S10. ^{1}H-NMR spectrum of $(DBPz)_2Ir(dpm)$.

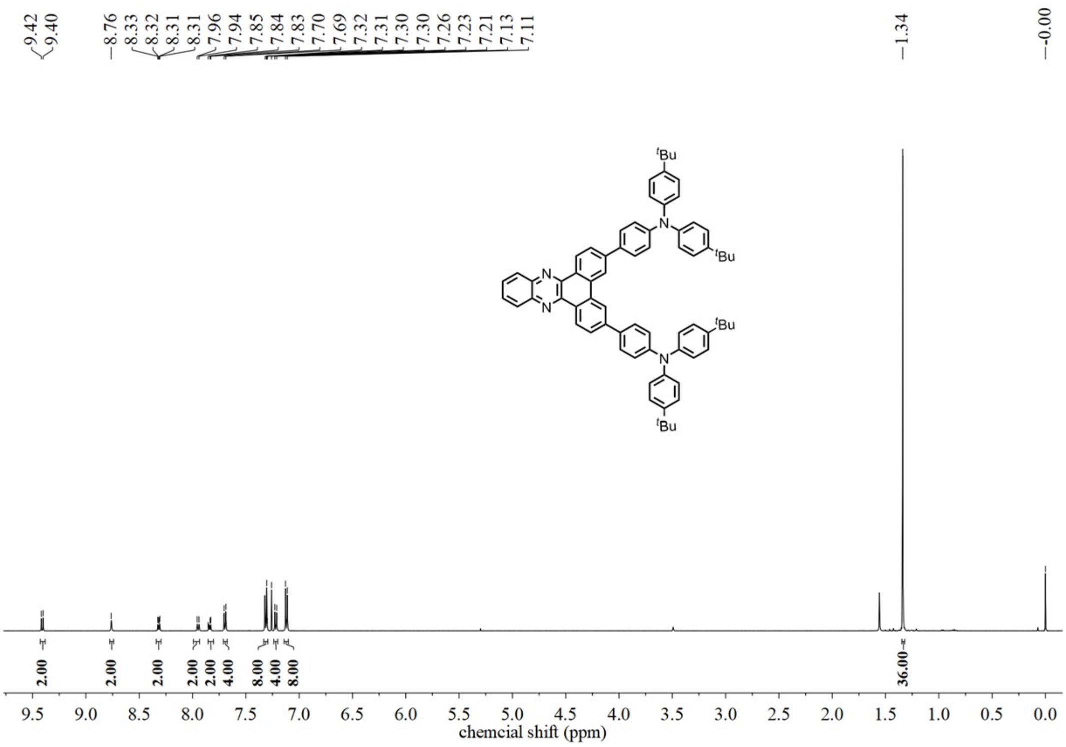

Figure S11. ^{1}H-NMR spectrum of ^{t}BuTPA-DBPzH.

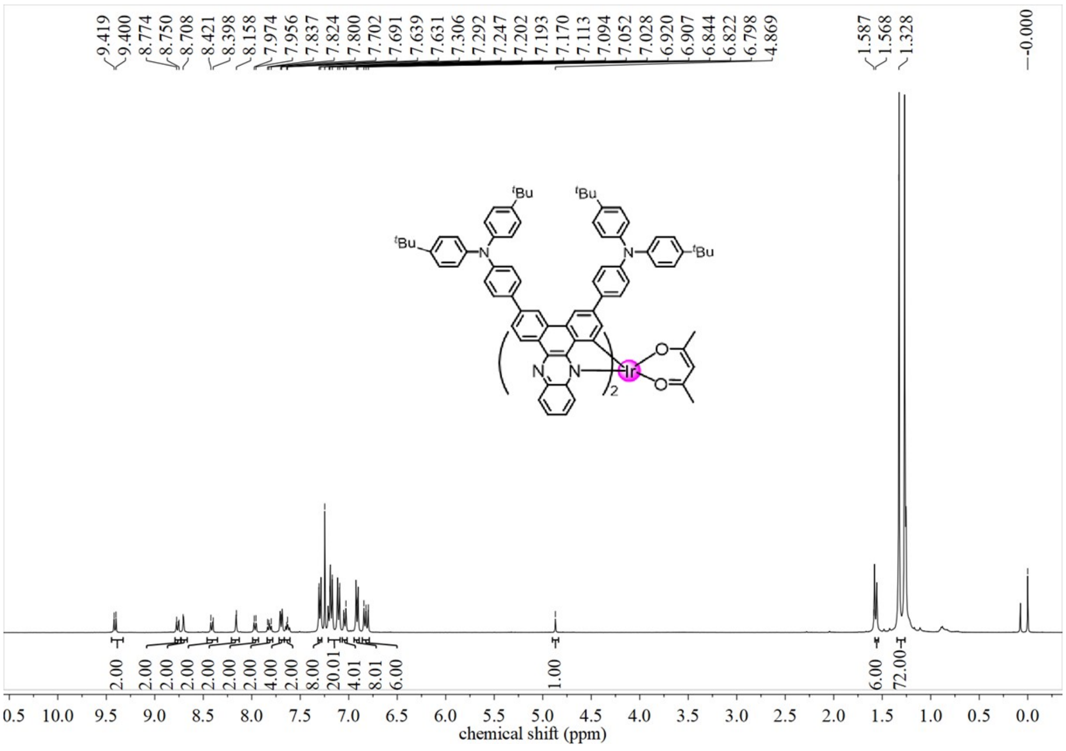

Figure S12. ^{1}H-NMR spectrum of (^{t}BuTPA-DBPz)$_2$Ir(acac).

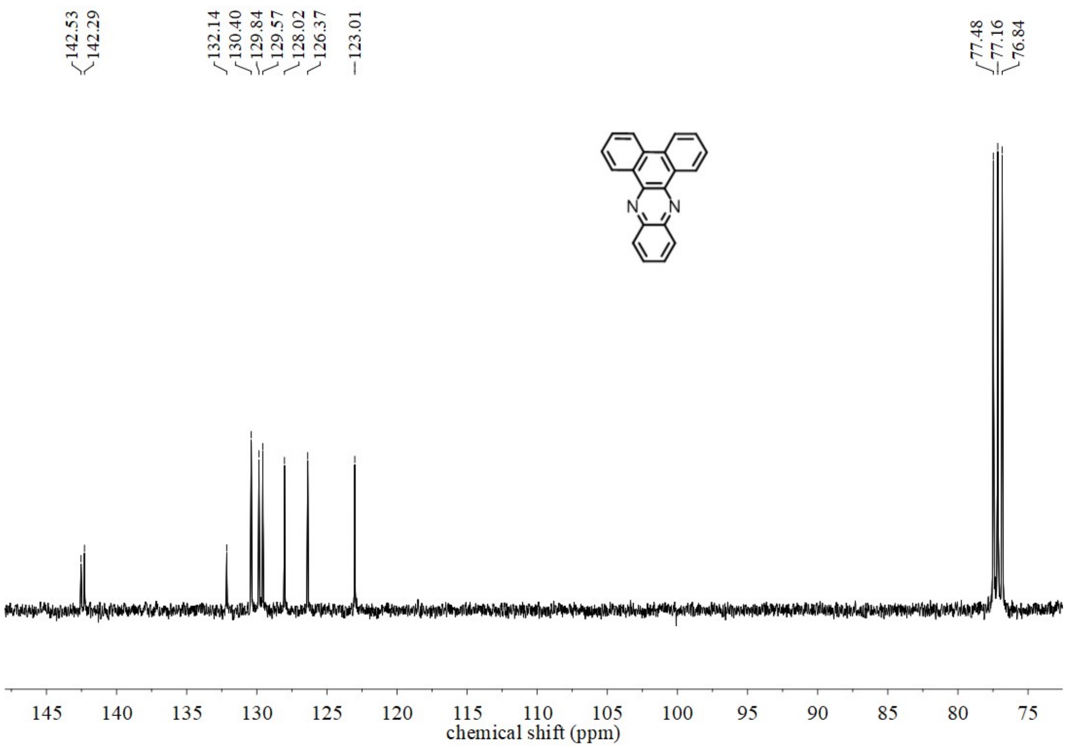

Figure S13.^{13}C-NMR of free ligand DBPzH.

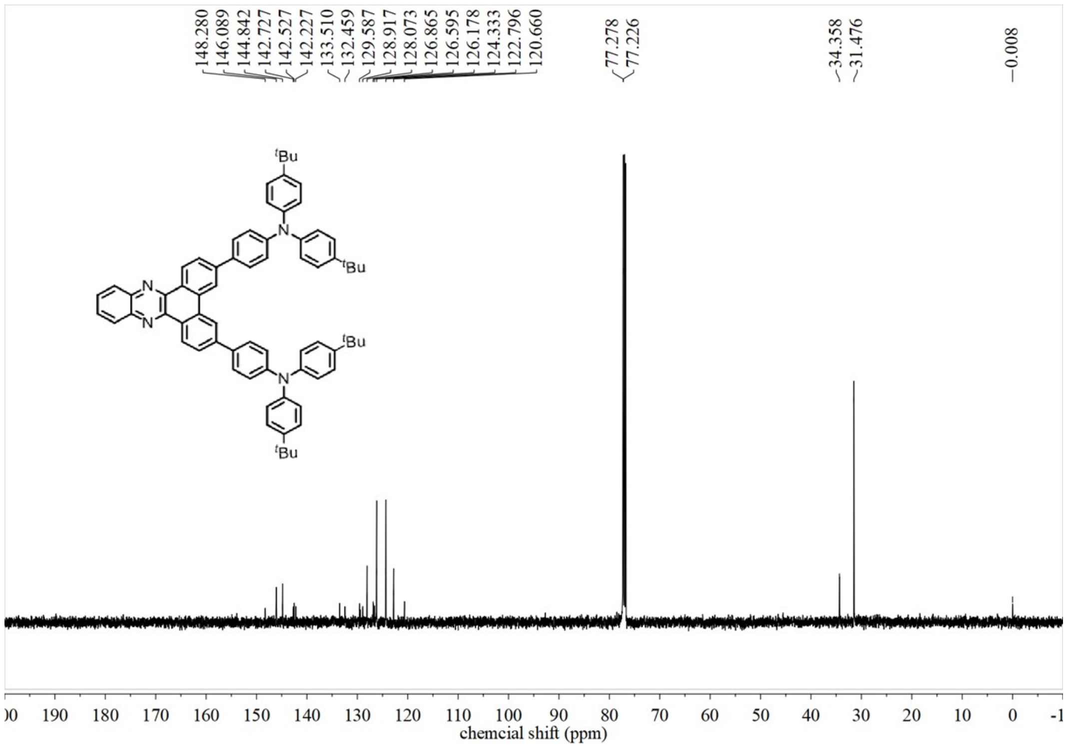

Figure S14.^{13}C-NMR of free ligand ^{t}BuTPA-DBPzH.

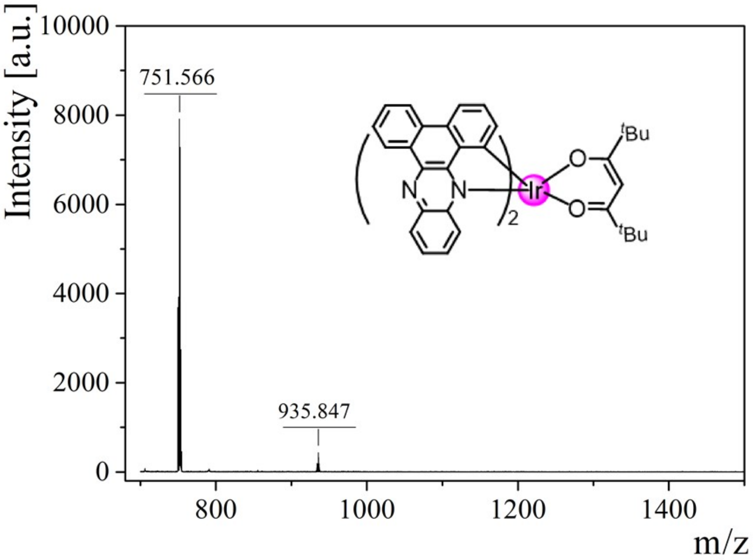

Figure S15.MALDI-TOF-MS spectrum of $(DBPz)_2Ir(dpm)$

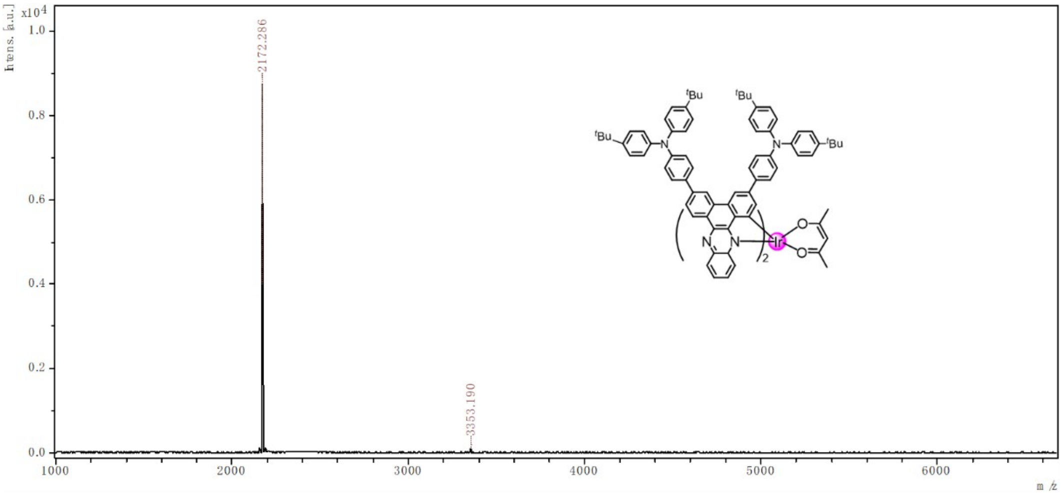

Figure S16.MALDI-TOF-MS spectrum of $({}^{t}BuTPA\text{-}DBPz)_2Ir(acac)$

Table S1. TD-DFT results for complexes based on their optimized S_0 geometries

complex		(DBPz)$_2$Ir(dpm)/%				(^{t}BuTPA-DBPz)$_2$Ir(acac)/%			
MOs [a]		L+1	L	H	H-1	L+1	L	H	H-1
contribution percentages of molecular moieties to MOs/%	Ir	3.92	3.00	37.29	25.98	4.15	2.68	0.59	0.54
	Main Ligand	95.69	96.42	58.26	11.79	95.48	96.83	99.28	99.43
	Auxiliary ligand	0.39	0.58	4.45	62.23	0.37	0.49	0.13	0.03
main configuration of $S_0 \rightarrow S_1$ excitation /E_{cal}/λ_{cal}/character [b]		H→L (97.4%) 2.04 eV 606 nm π(DBPz)/d_π(Ir)→π^*(DBPz)				H→L (95.31%) 1.99 eV 622 nm π(^{t}BuTPA-DBPz)/d_π(Ir)→π^*(^{t}BuTPA-DBPz)			
main configuration of $S_0 \rightarrow T_1$ excitation /E_{cal}/λ_{cal}/character [b]		H→L (94.39%) H-4→L+1 (2.6%) 1.80 eV 695 nm π(DBPz)/d_π(Ir)→π^*(DBPz)				H→L (84.9%) 1.76 eV 704 nm π(^{t}BuTPA-DBPz)/d_π(Ir)→π^*(^{t}BuTPA-DBPz)			

[a] H and L denote molecular orbitals (MO) HOMO and LUMO, respectively. [b] E_{cal} and λ_{cal} represent calculated excitation energies and corresponding wavelengths, data in parentheses are the contributions of corresponding excitations.

Table S2. Excited state properties of $(DBPz)_2Ir(dpm)$ obtained from TD-DFT calculations carried out at the ground state(S_0) geometry.

Complex	State（E, λ）	Dominant excitations	Oscillator strength	Character
$(DBPz)_2Ir(dpm)$	S_1 (2.04 eV, 606 nm)	HOMO→LUMO (97.4)	0.0039	ILCT/MLCT
	S_2 (2.06 eV, 601 nm)	HOMO→LUMO+1(95.2)	0.0401	ILCT/MLCT
	S_3 (2.37 eV, 523 nm)	HOMO-1→LUMO(84.56)	0.0365	ILCT/MLCT
	S_4 (2.45 eV, 505 nm)	HOMO-1→LUMO+1(83.57)	0.0000	ILCT/MLCT
	S_5 (2.82 eV, 438 nm)	HOMO-3→LUMO+1(10.58) HOMO-2→LUMO(84.11)	0.0688	ILCT/MLCT
	T_1 (1.80 eV, 695 nm)	HOMO-4→LUMO+1(2.6) HOMO→LUMO (94.39)	triplet	ILCT/MLCT
	T_2 (1.86 eV, 666 nm)	HOMO-4→LUMO (1.9) HOMO→LUMO+1 (92.6)	triplet	ILCT/MLCT
	T_3 (2.08 eV, 596 nm)	HOMO-3→LUMO (18.5) HOMO-1→LUMO (36.6)	triplet	ILCT/MLCT /LE
	T_4 (2.09 eV, 593 nm)	HOMO-2→LUMO (21.78) HOMO-1→LUMO+1(30.4)	triplet	ILCT/MLCT /LE
	T_5 (2.38 eV, 520 nm)	HOMO-2→LUMO+1(2.4) HOMO-1→LUMO (58.32)	triplet	ILCT/MLCT /LE

Table S3. Excited state properties of $({}^{t}$BuTPA-DBPz$)_2$Ir(acac) obtained from TD-DFT calculations carried out at the ground state(S$_0$) geometry.

Complex	State（E, λ）	Dominant excitations	Oscillator strength	Character
$({}^{t}$BuTPA-DBPz$)_2$Ir(acac)	S$_1$ (1.99 eV, 622 nm)	HOMO-4→LUMO(25.92) HOMO-1→LUMO(69.62) HOMO→LUMO (95.31)	0.0273	ILCT/MLCT
	S$_2$ (2.00 eV, 622 nm)	HOMO-1→LUMO+1(3.9) HOMO→LUMO (94.31)	0.0727	ILCT/MLCT
	S$_3$ (2.06 eV, 602 nm)	HOMO-4→LUMO(50.0) HOMO-2→LUMO(4.7) HOMO-1→LUMO(13.56) HOMO→LUMO+1(28.85)	0.0048	ILCT/MLCT
	S$_4$ (2.07 eV, 600 nm)	HOMO→LUMO+2(58.78) HOMO→LUMO+3(35.22)	0.1011	ILCT/MLCT
	S$_5$ (2.12 eV, 585 nm)	HOMO-4→LUMO(11.9) HOMO-2→LUMO(8.11) HOMO-1→LUMO(12.39) HOMO→LUMO+1(65.55)	0.0274	ILCT/MLCT
	T$_1$ (1.76 eV, 704 nm)	HOMO-1→LUMO(10.5) HOMO→LUMO (84.9)	triplet	ILCT/MLCT
	T$_2$ (1.80 eV, 688 nm)	HOMO-4→LUMO+1(39.81) HOMO→LUMO (54.06)	triplet	ILCT/MLCT
	T$_3$ (1.91 eV, 646 nm)	HOMO-4→LUMO+1(16.5) HOMO→LUMO (30.96)	triplet	ILCT/MLCT /LE
	T$_4$ (1.93 eV, 642 nm)	HOMO-2→LUMO (15.1) HOMO→LUMO+1(19.5)	triplet	ILCT/MLCT /LE
	T$_5$ (2.02 eV, 611 nm)	HOMO-3→LUMO (21.12) HOMO-1→LUMO+1(13.37) HOMO→LUMO (33.79)	triplet	ILCT/MLCT /LE

Table S4 EL performance of the $({}^{t}$BuTPA-DBPz$)_2$Ir(acac) doped devices at different dopant ratios.

Dopant	Ratio (wt %)	V_{on}[a] (V)	λ_{EL}[b] (nm)	$EQE_{\max}$[c] (%)	$R_{\max}$[d] (mW/Sr/m^2)
$(^{t}\text{BuTPA-DBPz})_2\text{Ir(acac)}$	1.0 wt%	6.4	710	4.50	21063
	4.0 wt%	7.2	714	10.11	32847
	8.0 wt%	8.0	714	12.25	45326

[a] Turn-on voltage. [b] The maximum EL emission peak. [c] The maximum external quantum efficiency. [d] Radiant intensity.

Experimental section

Materials

Unless otherwise specified, most of the solvents and reagents are commercially available (TCI, energy chemical) and used without further purification. All reactions were conducted under a N_2 atmosphere using the standard Schlenk line techniques to avoid the oxidation of the reactants by oxygen. The toluene and dichloromethane were dried and distilled according to the common methods before used. Column chromatography was carried out with Merck silica gel (200 - 300 mesh). Thin-layer chromatography (TLC) was adopted to inspect reactions until the reactants were fully consumed.

Instrumentation

NMR spectra (^{1}H) was recorded at RT on a Bruker Avance III spectrometer at 400 Hz for ^{1}H-NMR, which using $CDCl_3$ as solvent and tetramethyl silane (TMS) signals as the internal standard. Mass spectra (MS) results were performed on a Bruker Auto flex MALDI TOF instrument. Elemental analyses are performed on the Vario EL III instrument. The UV–Vis absorption and photoluminescence (PL) spectra were obtained on a Shimadzu UV-2600 and Perkin-Elmer LS45 luminescence spectrometer, respectively. Phosphorescence decay lifetimes were measured on an Edinburgh FLS1000 Spectrometer with time-corrected single-photon-counting (TCSPC) measurement after removing the oxygen in the solution by vacuum technique (three freeze-pump-thaw cycles). Low temperature phosphorescence spectra were performed in film at 77 K on Edinburgh FLS1000 Spectrometer. The photoluminescence quantum yields (PLQYs) of iridium complex were measured in degassed DCM solutions using $(\text{DBQ})_2\text{Ir(acac)}$ as standard (Φ_{P}=0.53, in DCM solution at 298 K, λ_{ex}=370 nm)[1]. PLQYs was calculated using the equation of $\Phi_{\text{s}}=\Phi_{\text{r}}(\eta_{\text{s}}^2 I_{\text{S}} A_{\text{r}}/\eta_{\text{r}}^2 I_{\text{r}} A_{\text{s}})$, where Φ stands for the quantum yield, η is the refractive index of the solvent, A is the absorbance of the sample or the reference at the wavelength of excitation, and I presents the integrated areas of emission bands, subscript ‘‘s” and ‘‘r” represents sample and reference, respectively.[2] Cyclic voltammetry (CV) was performed using CHI630E at a scan rate of 100 mV s^{-1}. All experiments were carried out in a three-electrode compartment cell with a Pt-wire counter electrode, a Pt-disk working electrode and Ag/AgCl reference electrode. The supporting electrolyte used was 0.1 M tetrabutylammonium hexafluorophosphate ([Bu_4N]PF_6) solution in dry HPLC grade acetonitrile under a nitrogen atmosphere using ferrocene (Fc) as the calibrant. The HOMO and LUMO levels are calculated by assuming the energy level of ferrocene/ferrocenium to be -4.8 eV. The thermal gravimetric analysis (TGA) was performed on a TA Instruments (TGA 50) under nitrogen gas flow with a heating rate of 20 °C min^{-1}.

All calculations were carried out with Gaussian 09 software package using a spin-restricted formalism. The ground states of the complexes were calculated using density functional theory (DFT) and time-dependent DFT (TD-DFT) at the B3LYP/6-31G(d)/LanL2DZ level.

Preparation of NIR-OLEDS

The structure of doped device is ITO/PEDOT: PSS(35 nm)/CBP: dopants (X wt%,40 nm or 50 nm) /TmPyPB(50 nm)/LiF(0.5 nm)/Al (120 nm),Wherein, ITO act as anode. PEDOT: PSS acted as hole-injection layer (HIL), respectively. CBP is a superior host with a favorable electron trapping character, which was reported as a multifunctional material with extraordinary hole injection ability and high hole/electron mobilities. TmPyPB acts as an electron-transporting layer (ETL) and a hole blocking layer (HBL). LiF was used as an electron-injection layer (EIL) and Al acts as a cathode. PEDOT: PSS were spin coated on precleaned ITO glass substrates and annealed at 160 °C for 20 min (thickness: 35 nm). Subsequently, the blend of CBP and dopants in chlorobenzene solution was spin coated directly on top of the PEDOT: PSS (thickness: 40 nm or 50 nm) as the light emitting layer. Finally, TmPyPB films (thickness of 50 nm) were then spin-coated on the active layer. Finally, LiF/Al electrodes were thermally evaporated through a shadow mask. The active area of the OLEDs was 4 mm^2. In order to avoid degradation and emission quenching caused by oxygen and moisture, all OLEDs were encapsulated in a glove box prior to the device characterization.

OLEDs measurements:

The EL spectra and current density (J)-voltage (V)-luminance (L) curves were obtained using a PHOTO RESEARCH Spectra Scan PR 745 photometer and a KEITHLEY 2400 Source Meter constant current source at room temperature. The *EQE* values were done by calculation.

Synthesis

General synthesis procedure for Schiff-base condensation reaction.

A mixture of 1 equiv compound phenanthrene-9,10-dione or 3,6-dibromophenanthrene-9,10-dione and 1 equiv o-phenylenediamine in absolute ethanol with catalytical amount of acetic acid were heated to reflux for 8 h under vigorous stirring. After cooling to RT, two different yellow solids were obtained after filtration. Further purified by a flash silica gel column using petroleum ether/dichloromethane mixture as the eluent to give the desired product DBPzH and M1.

DBPzH: ^{1}H NMR (400 MHz, $CDCl_3$) δ (ppm): 9.45 – 9.39 (m, 2H), 8.58 (d, J = 7.9 Hz, 2H), 8.34 (dd, J = 6.5, 3.4 Hz, 2H), 7.87 (dd, J = 6.5, 3.4 Hz, 2H), 7.83 – 7.72 (m, 4H). ^{13}C NMR (100 MHz, $CDCl_3$) δ (ppm): 142.53, 142.29, 132.14, 130.40, 129.84, 129.57, 128.02, 126.37, 123.01. Anal. Calcd for $C_{20}H_{12}N_2$: C, 85.69; H, 4.31; N, 9.99. found: C, 85.86; H, 4.71; N, 10.02.

Synthesis of ^{t}BuTPA-DBPzH

Under nitrogen atmosphere, a mixture of 1 equiv intermediate M1, 2.5 equiv of (4-(diphenylamino)phenyl)boronic acid, 0.04 equiv of $Pd(PPh_3)_4$ were dissolved into toluene, then an aqueous solution of K_2CO_3 (2 M, 8 equiv) and 1.0 mL ethanol were added, the resulting reaction mixture were heated at 80 °C for 12 h, after the completely consumption of the staring materials (monitored by TLC), the reaction mixture was cooling to room temperature and washed with brine, extracted with dichloromethane (2×20 mL). The combined organic phase was dried over anhydrous Na_2SO_4 and solvent was removed under reduced pressure. The crude mixture was then purified by chromatography on silica gel with petroleum ether/dichloromethane mixture as eluent to furnish ligand ^{t}BuTPA-DBPzH as bright yellow solid, 80% yield.

^{t}BuTPA-DBPz : ^{1}H NMR (500 MHz, $CDCl_3$) *δ* 9.41 (d, J = 8.4 Hz, 2H), 8.76 (s, 2H), 8.32 (dd, J = 6.5, 3.4 Hz, 2H), 7.95 (d, J = 8.4 Hz, 2H), 7.83 (d, J = 3.4 Hz, 2H), 7.70 (d, J = 8.6 Hz, 4H), 7.33 – 7.29 (m, 8H), 7.22 (d, J = 8.6 Hz, 4H), 7.12 (d, J = 8.6 Hz, 8H), 1.35 – 1.32 (m, 36H). ^{13}C NMR (126 MHz, $CDCl_3$) δ 148.28, 146.09, 144.84, 142.73, 142.53, 142.23, 133.51, 132.46, 129.59, 128.92, 128.07, 126.87, 126.60, 126.18, 124.33, 122.80, 120.66, 77.28, 77.23, 34.36, 31.48, 0.01.

Synthesis of iridium(III) μ-chloro-dimer complexes

Under N2 atmosphere, 1 equiv of chloro(1,5-cyclooctadiene)iridium(I) dimer $[IrCl(COD)]_2$ and 4 equiv of ligand DBPzH or ^{t}BuTPA-DBPzH were refluxed at 115 °C for 40 h in 20 mL toluene. The reaction mixture was slowly turned to dark black. Toluene is removed off under reduced pressure and the iridium(III) μ-chloro-dimer were used directly for the next reaction.

Synthesis of (DBPz)$_2$Ir(dpm) and (^{t}BuTPA-DBPz)$_2$Ir(acac)

1 equiv of the corresponding μ-chloro-dimer, 2 equiv of acetylacetone (acacH) or 2,2,6,6-Tetramethyl-3,5-Heptanedione (dpmH) and 2.5 equiv of ^{t}BuOK were added into the mixture of dichloromethane and methanol [20 mL, 3/1 (V/V)]. Then the reaction mixture was refluxed at 40 °C under N_2 atmosphere overnight. After cooling down to room temperature, the mixture was extracted with dichloromethane and washed by distilled water. The solution was dried over anhydrous Na_2SO_4 and the solvent is evaporated to dryness. The residual was purified by flash column chromatography using petroleum ether/dichloromethane as the eluent to get dark black solid (DBPz)$_2$Ir(dpm) and (^{t}BuTPA-DBPz)$_2$Ir(acac), the yields were 30% and 37%, respectively. The dark black solid were recrystallized from methanol and dichloromethane mixture, followed by vacuum drying process to provide iridium(III) complex before characterization.

(DBPz)$_2$Ir(dpm): ^{1}H NMR (400 MHz, $CDCl_3$): *δ* (ppm) 9.45 (d, *J* = 7.6 Hz, 2H), 8.59 (d, *J* = 8.7 Hz, 2H), 8.52 (d, *J* = 7.8 Hz, 2H), 8.41 (d, *J* = 8.4 Hz, 2H), 7.96 (d, *J* = 7.8 Hz, 2H), 7.86 – 7.76 (m, 6H), 7.55 (t, *J* = 7.8 Hz, 2H), 6.98 (t, *J* = 7.7 Hz, 2H), 6.65 (d, *J* = 7.5 Hz, 2H), 5.13 (s, 1H), 0.53 (s, 18H). MS (MALDI-TOF, m/z) $[M+1]^+$ calcd for $C_{51}H_{41}IrN_4O_2$ 935.13, found 935.84.

(^{t}BuTPA-DBPz)$_2$Ir(acac): ^{1}H NMR (400 MHz, $CDCl_3$) δ 9.41 (d, J = 7.7 Hz, 2H), 8.76 (d, J = 9.5 Hz, 2H), 8.71 (s, 1H), 8.41 (d, J = 9.5 Hz, 3H), 8.16 (s, 3H), 7.97 (d, J = 7.2 Hz, 2H), 7.84 – 7.78 (m, 3H), 7.70 (d, J = 4.1 Hz, 3H), 7.63 (d, J = 3.5 Hz, 2H), 7.30 (d, J = 5.9 Hz, 7H), 7.21 – 7.09 (m, 5H), 7.04 (d, J = 9.5 Hz, -1H), 6.91 (d, J = 5.3 Hz, 2H), 6.86 – 6.79 (m, -2H), 4.87 (s, 0H), 1.57 (s, 4H), 1.33 (s, 61H).MS (MALDI-TOF) [M-acac]$^+$: calcd for $C_{144}H_{138}IrN_8$: 2172.07; found: 2172.96

References

[1] J.P. Duan, P.P. Sun, C.H. Cheng, Adv. Mater. 2003, **15**, 224-228.
[2] Jian L I, Djurovich, Peter I, et al. Inorg.Chem, 2005, **44**,1713-1727.